Journal of Testing and Evaluation

doi:10.1520/JTE20190650 / Vol. 48 / No. 3 / 2020 / available online at www.astm.org

Zejiao Dong,[1] Tongxu Wang,[2] Xianyong Ma,[2] Cheng Cao,[3] Fandong Kong,[3] and Zhen Leng[4]

Dynamic Response Analysis of Airport Asphalt Pavement Subjected to High-Temperature Jet Wake Based on Finite Element Simulation

Manuscript received April 3, 2019; accepted for publication February 21, 2020; published online March 19, 2020. Issue published May 1, 2020.

[1] School of Transportation Science and Engineering, Harbin Institute of Technology, No. 73 Huanghe Rd., Nangang District, Harbin 150090, Heilongjiang, PR China (Corresponding author), e-mail: hitdzj@hit.edu.cn, https://orcid.org/0000-0002-2115-3802

[2] School of Transportation Science and Engineering, Harbin Institute of Technology, No. 73 Huanghe Rd., Nangang District, Harbin 150090, Heilongjiang, PR China

[3] Beijing Capital International Airport Company Limited, No. 2 Lusheng Rd., Beijing Airport Logistics Park, Shunyi District, Beijing 100621, PR China

[4] Department of Civil and Environmental Engineering, The Hong Kong Polytechnic University, 181 South Chatham Rd., Hung Hom, Kowloon, Hong Kong, PR China

Reference

Z. Dong, T. Wang, X. Ma, C. Cao, F. Kong, and Z. Leng, "Dynamic Response Analysis of Airport Asphalt Pavement Subjected to High-Temperature Jet Wake Based on Finite Element Simulation," *Journal of Testing and Evaluation* 48, no. 3 (May/June 2020): 1876–1892. https://doi.org/10.1520/JTE20190650

ABSTRACT

With the dramatic increase of air traffic volume and the rapid development of civil aviation airport construction in China, asphalt layers overlaying original concrete pavement in civil aviation airports has become the primary rehabilitation scheme. However, asphalt airport pavement is prone to excessive deformation when subjected to the repeated and heavy aircraft loading, especially when coupled with high-temperature field. However, the impact of high-temperature jet wake is rarely considered in the existing structural design and analysis of airport asphalt pavement. In order to investigate the impact of high-temperature jet wake on the dynamic response of asphalt pavement, the coupling of finite element (FE) simulation of the temperature field and aircraft loading based on sequential decoupling methodology was implemented herein. Firstly, the temperature field distribution induced by the high-temperature jet wake on the asphalt pavement was simulated and analyzed by FE simulation on the ABAQUS CFD platform. Then, the temperature field distribution was integrated within the asphalt pavement structure by combining the temperature field distribution produced by jet wake and thermal conduction between ambient radiation and pavement. Secondly, the viscoelastic parameters of each asphalt layer under the obtained temperature field distribution were calculated to represent more real material properties. Finally, FE simulation of airport asphalt pavement subjected to the coupling of aircraft loading and integrated temperature field was conducted. The results show that the amplitudes of transverse strain, vertical strain, and longitudinal strain of the asphalt pavement considering jet wake together with ambient radiation are basically higher than those without consideration. Consequently, the dynamic

responses of airport asphalt pavement produced by jet wake and ambient radiation should be fully considered in the design and analysis of airport asphalt pavement.

Keywords

airport asphalt pavement, jet wake, integrated temperature field, aircraft loading, numerical simulation

Introduction

In recent years, civil aviation airport construction in China has been developing continuously and rapidly because of the dramatic increase in air traffic volume. According to the statistical data released by National Data Network, the annual passenger throughput of Beijing Capital International Airport has reached 95.786 million in 2018, ranking the first in Asia and the second globally. With the increasing demand of passenger throughput capacity, the airport is also introducing advanced technologies, such as Internet of Things, cloud computing, and efficient information system control, to improve its operational efficiency, management capacity, and service level.[1]

Because of the harsh strength and stability requirement of airfield pavement, cement concrete pavements were commonly built in the early years in most mainland airports. Under the long-term actions of the external environment and heavy aircraft loading, the service performance declined rapidly and there was some structural damage, which seriously affected the safety of airports. In addition, with the rapid development of aviation technology and economic growth, new large passenger aircraft are constantly coming out, such as Airbus 380, Boeing 787, and COMAC 919; this has caused a rapid increase in airport traffic volume. In order to meet the requirements of nonstop construction, asphalt overlays are utilized by more and more airports in China to reinforce the existing cement concrete pavement. According to the statistical data of the International Civil Aviation Organization and the European Asphalt Pavement Association, asphalt concrete pavement has been adopted by many large civil and military airports worldwide because it allows for comfortable driving, produces very little aircraft vibration, and permits convenient construction and maintenance.[2]

However, asphalt airport pavement is inevitably affected by environmental factors like temperature, solar radiation, and wind power, resulting in complicated and changeable temperature field distribution within the pavement. However, temperature condition has a significant impact on the bearing capacity and service performance of asphalt pavement because of the inherent viscoelastic characteristics of asphalt material. Under the coupling of temperature and loading, many asphalt pavements have distresses dominated by rutting and fatigue damage. For the analysis of pavement temperature field, there are three main methods: analytical method, numerical simulation method, and statistical regression method. In 1988, the SHRP program was launched in the United States. Firstly, the performance of asphalt and asphalt mixture was proposed according to the climate division plan, and a huge database of pavement temperature and meteorological data were established, which provided a data foundation for the establishment of performance models.[3] A computer tool (CalCool) was created based on the considerations of theoretical heat transfer for pavement designers and on-site construction crews to predict pavement temperature during construction and modify designs or compaction procedures accordingly.[4] Based on the surface energy balance method, Feng and Feng[5] established a road surface temperature prediction model using solar shortwave radiation, longwave radiation, sensible and latent heat fluxes, and surface heat flux. Chen, Wang, and Zhu[6] put forward an analytical solution of temperature fields in the multilayered pavement structure, which was derived with the Green's Function method by using climatic factors including solar radiation, wind velocity, and air temperature as input parameters. Some scholars also established models through analytical methods to predict temperature fields in rigid and flexible pavement.[7–9] The relative effects of different thermal properties on the pavement surface were simulated by Gui et al.[10] A transient, two-dimensional finite-difference model was developed to predict asphalt pavement temperature at different depths and horizontal locations based on thermal environmental conditions, which greatly helped pavement engineers in performing back-calculations of pavement modulus values and selecting the asphalt grade.[11] By means of field measurement

and numerical simulation, the transient behavior of asphalt concrete pavement and the temperature at different levels of bituminous layers were simulated by Minhoto et al.[12] Diefenderfer, Al-Qadi, and Diefenderfer[13] established a model for estimating the rutting performance given heavy vehicle loading and low-temperature cracking of hot mix asphalt pavements through statistical regression analysis. Also, the prediction model for predicting mid-depth temperature for perpetual (thicker) asphalt pavements was developed.[14]

The coupled effect of temperature and stress loading is the primary cause of the deformation and failure of the pavement structure.[15] Based on the thermoviscoelastic deformation theory of asphalt mixtures, a lot of research have been done on the combined effects of the constitutive model and temperature on dynamic responses of asphalt pavement's stress-strain under moving wheel loads.[16,17] However, most researches were based on the conditions of highways to predict the long-term rutting law in asphalt pavement design life without considering the rutting development under the specific environmental and loading conditions like airports, especially under the short-term sustained high-temperature and heavy loading conditions.[18–20] As an important part of the aircraft propulsion system, in order to obtain enough thrust when taxiing or taking off, an engine exhaust device will generate a huge amount of high-temperature exhaust gas instantaneously. Therefore, the influence of high-temperature jet wake generated by an aircraft engine during the take-off, landing, and taxiing stages on the temperature field of pavement surface could not be negligible. It is generally believed that aircraft wake could be divided into three parts: wing tip vortex, boundary layer turbulence, and engine turbulence. Among them, the wingtip vortex has a great impact on aircraft flight safety, as has been confirmed by numerous studies. Comparatively, research focusing on engine turbulence is relatively scarce. Since the late 20th century, Crow[21] has been studying the development and dissipation process of the near-surface jet wake; therefore, Crow instability theory was developed. The distribution of temperature and pressure behind the tail nozzle of the engine through the jet flow field test and jet blast deflector or blast fence test was measured.[22] According to the Somani's hypothesis, Ahyudanari, Shafiq, and Kamaruddin[23] obtained the thermal loading paths of A319 and B737. A particular system was developed to measure the temperature distribution of jet wake under the full force of the engine.[24] However, the aforementioned investigations are based on field measurements of specific types of aircrafts. Moreover, the policy limitations of airport management make it difficult to measure. There are few investigations that focus on the combined temperature distribution from jet wake and normal environment and its effect on the dynamic response of asphalt airport pavement. As a result, the ABAQUS CFD platform was utilized to simulate and analyze the temperature distribution of high-temperature jet wake, and the mechanical response of airport asphalt pavement induced by the coupling of aircraft loading and temperature field was explored herein.

Decoupling Methodologies of Numerical Simulation

Two main sources of thermal input on airport asphalt pavement are considered in this article. One is ambient radiation, which primarily refers to the solar radiation, the convective heat transfer between the asphalt pavement and the outside, and pavement surface radiation. The other is the "centralized heating effect" of high-temperature jet wake from an aircraft engine on the pavement surface when the aircraft is taxiing or waiting for the next operational instruction on the pavement temporarily. **Figure 1** illustrates the structure and working principle of a civil turbofan jet engine. To make an aircraft move forward, 80 % of engine airflow accelerated by the fan on the propeller goes directly into the bypass duct and provides 80 % of the thrust of the engine. The primary flow passes in succession through the low-pressure, high-pressure compressors, combustor, and turbines before being injected rearward through the exhaust assembly. After entering the combustion chamber, burning the mixture of fuel and air brings the temperature to 1,700°C. Finally, the thermal energy after combustion is converted into the mechanical energy of the turbine, and the fan and compressor are driven by a concentric shaft to realize the cycle engine.

According to the research by Yu, Shi, and Deng,[24] when the engine is operating at full force state, the jet wake core temperature could reach up to 1,500°C~1,800°C. While in the intermediate state, the core zone is 0.4~4 m

FIG. 1

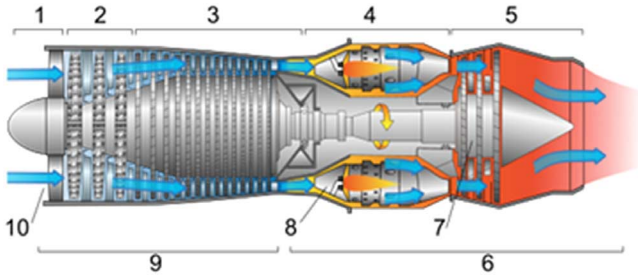

The configuration of a turbofan jet engine. 1. Propeller. 2. Low-pressure compressors. 3. High-pressure compressors. 4. Combustion chamber. 5. Nozzle. 6. Hot side. 7. Turbine. 8. Burners. 9. Cold side. 10. Inlet port.

away from the nozzle, and the temperature reaches 500°C~600°C. Therefore, the temperature analysis of high-temperature jet wake is also extremely important.

Figure 2 presents the sequential decoupling scheme for dynamic response analysis because of the combined jet wake and ambient radiation on asphalt airport pavement based on finite element (FE) simulation. As a typical analysis case, the B737 aircraft was studied herein. Based on the proposed sequential decoupling scheme, the simulation was started with the temperature field distribution that was brought by the high-temperature jet wake on the pavement surface, and then the integrated temperature field distribution of jet wake and ambient radiation within the pavement structure was qualitatively investigated. Next, the viscoelastic parameters of asphalt mixture, depending on local temperature, were set by the Prony series and Williams-Landel-Ferry (WLF) equation in ABAQUS. Finally, dynamic response variation inside pavement structure under the coupling of temperature and aircraft loading was studied and compared with those of only aircraft loading. The research herein lays the foundation for the subsequent rutting analysis of airport asphalt pavement.

FIG. 2 Flowchart of a sequential decoupling scheme.

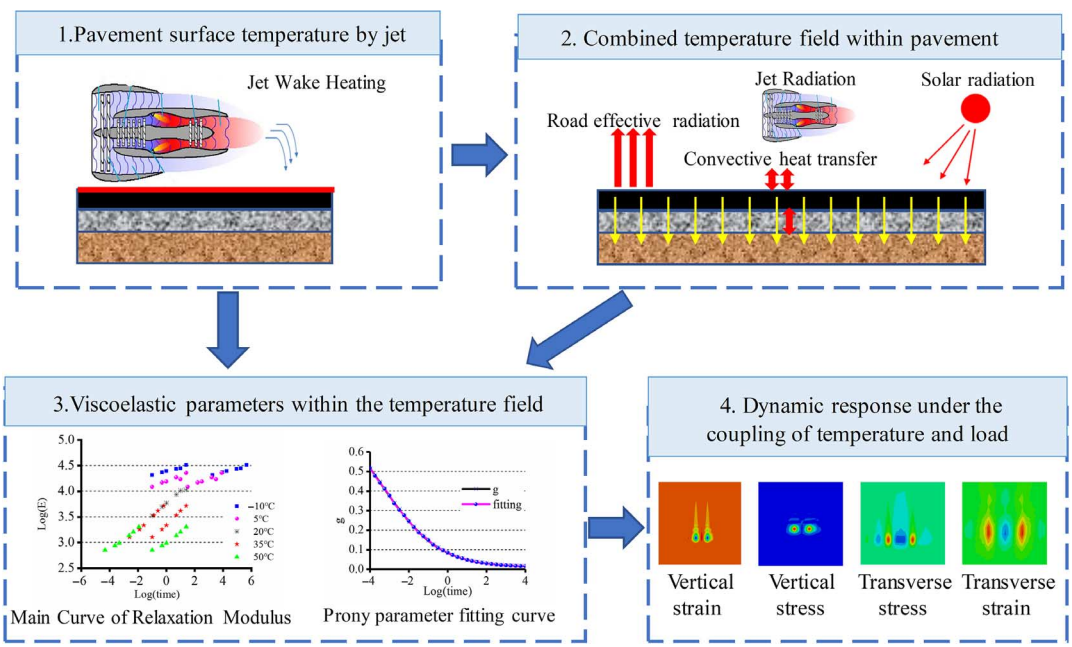

Integrated Temperature Field of Pavement Structure

THE TEMPERATURE FIELD OF PAVEMENT SURFACE INDUCED BY JET WAKE

Parameters Determination

According to Wang et al.,[22] there is no superposition of temperature and pressure between the twin engines of an aircraft. Consequently, one jet wake was analyzed considering the symmetry of the investigated model. Figure 3 shows the meshing of the flow field model outside the tail nozzle, a total of 154,000 elements. The diameter of the nozzle outlet and the external flow field are 1 m and 12 m, respectively, and the length is 60 m. The center of the tail nozzle is 1.3 m away from the pavement surface; thus, the bottom boundary of the tail nozzle outlet is 0.8 m from the pavement. In order to facilitate subsequent results analysis, a coordinate system is established as shown in figure 3*A*, and the origin is set on the pavement surface corresponding to the center of the tail nozzle outlet, which is shown in figure 3*B*.

Structured meshing methodologies were adopted, which were partially encrypted at the nozzle outlet and transited to coarse grids along the radial and axial directions gradually. The initial condition of the nozzle outlet was 500°C, the velocity of jet wake was 0.8 Ma. The pressure boundary condition of the external flow field was standard atmospheric pressure, and the ambient temperature was 30°C. Flow wall boundary condition was adopted at the pavement surface.

Nodes temperature could be calculated by the thermal analysis module of ABAQUS platform based on the heat balance equation of the energy conservation principle, and other thermal characteristics parameters could be derived. Table 1 presents the thermal characteristic parameters of jet wake at 30°C and 101.325 KPa.

Result Analysis

According to the results of 0.8 s, the temperature in the core zone of jet wake at 15, 20, 30, 40, 50, and 60 m from the nozzle were analyzed here. Figure 4*A* gives the temperature distribution on pavement surface under the

FIG. 3 The meshing model of the flow field: (*A*) the global model; (*B*) detail dimension and meshing.

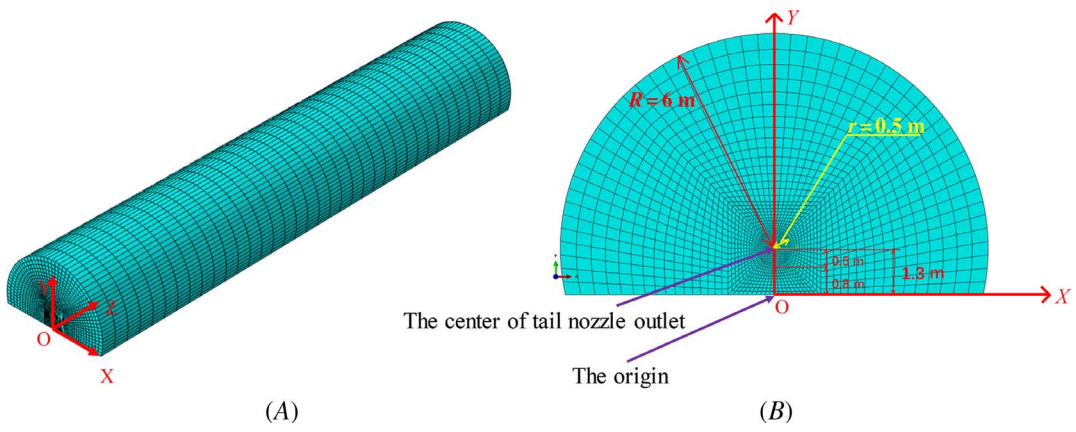

TABLE 1
Thermal parameters of jet wake

Jet Wake, 30°C, 101.325 KPa	Density, kg/m^3	Specific HeatCp, J/kg·K	Conductivity, J/mh·°C	Thermal Expansion Coefficient, °C^{-1}	Dynamic Viscosity, Pa·s
Value	1.1516	1,020.5	0.023	0.00366	1.87e-05

FIG. 4 Temperature field distribution and temperature curves at different distances: (*A*) temperature field distribution; (*B*) temperature curves at different distances.

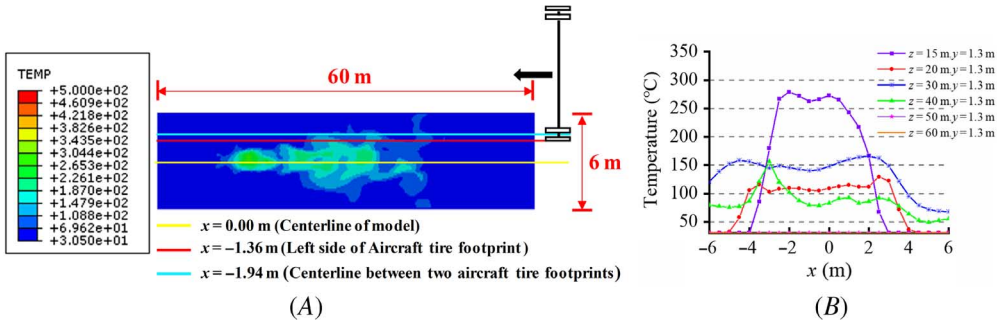

action of jet wake from B737 aircraft. Figure 4*B* presents the temperature in the core zone of jet wake, which is higher in the range of 2~4 m from the centerline, and the maximum temperature reaches 200°C~300°C. As can be seen from figure 5, the temperature of jet wake gradually decreases along the ejection direction, and the rate of decrease within 0.4 s is about 44.6 %. Figure 6 shows the temperature distribution at the position of aircraft tire footprint on pavement surface.

According to the symmetric characteristics of temperature distribution at the bottom of the flow field, five groups of node temperatures at the aircraft tire footprint are analyzed. It can be found from figures 5 and 6 that the temperature on the pavement surface ($y = 0$ m) is higher in the range of 7.2–43.2 m away from the outlet of the nozzle, and the maximum temperature of the centerline reaches 286.9°C. The maximum temperature on three paths (i.e., $x = -1.36$ m, $x = -1.51$ m and $x = -1.94$ m) are 200.4°C, 177.9°C, and 152.6°C, respectively. Therefore, the pavement surface temperature field, which is due to the high-temperature jet wake, has a significant influence on the central and surrounding areas of aircraft tire footprints. Actually, the impact of high-temperature jet wake on the pavement surface is reduced by factors like aircraft speed, wind speed, and real-time ambient temperature. Therefore, an adverse case was chosen in hot weather on June 4 in Beijing, considering the temperature at the center of the aircraft tire footprint affected by the high-temperature jet wake. The ultimate time history of pavement surface temperature is shown in figure 7 as the input of subsequent integrated temperature distribution analysis, which illustrates the temperature field within asphalt pavement structure. The red dotted line represents the hourly temperature on June 4th, and the black line represents the ultimate time history with the consideration of the effect of jet wake at 1.51 m.

FIG. 5

Temperature distribution at 0.4 s.

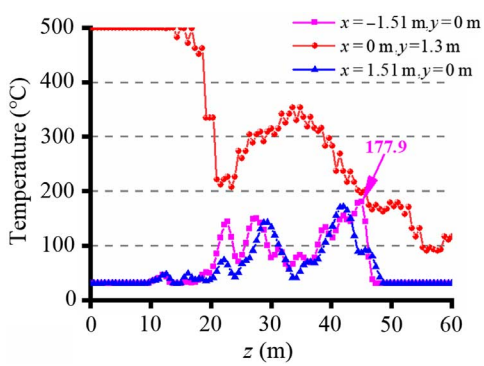

FIG. 6

Temperature distribution of pavement surface.

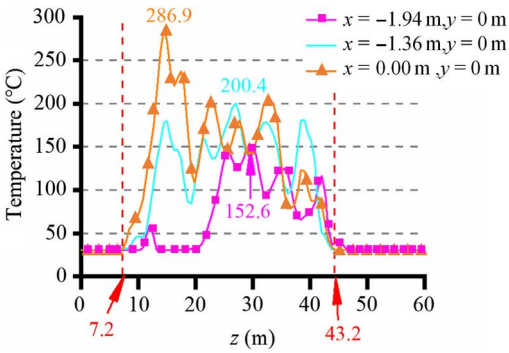

FIG. 7 The ultimate time history of pavement surface temperature.

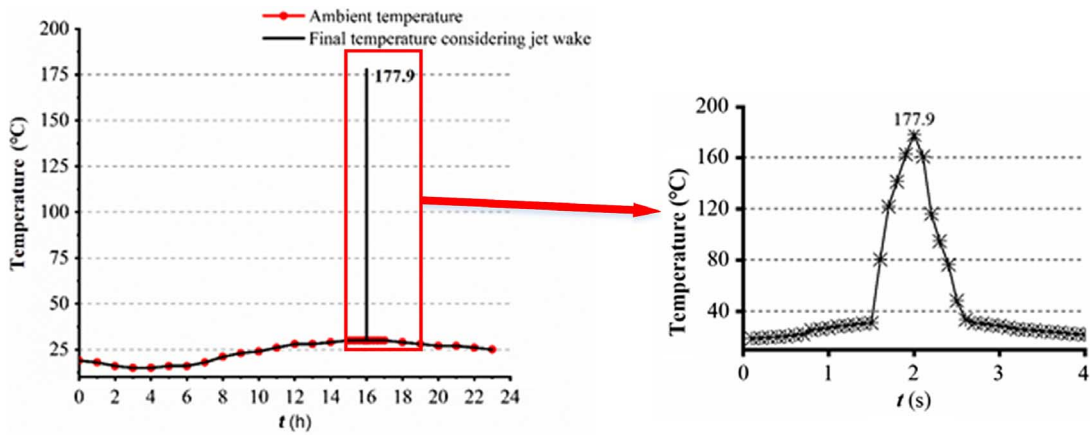

THE TEMPERATURE FIELD INSIDE THE ASPHALT PAVEMENT

Parameters Determination

The temperature field model of the two-dimensional pavement structure was established without considering the change of material parameters with temperature. Thermal characteristic parameters of the pavement structure are shown in Table 2. The main factors affecting the temperature field inside the asphalt pavement are shown in Table 3, including the daily average maximum temperature, daily average minimum temperature, daily average wind speed, effective sunshine time (t_1), time of jet wake acts on pavement (t_2), and total solar radiation.

The two-dimensional thermal model is 10 m in length and 5 m in height. The structural meshing is shown in figure 8, which is partially encrypted at an aircraft tire footprint and upper pavement structure to coarse grids along the radial and lateral directions gradually. Concurrently, they are consistent with the three-dimensional model meshing of the dynamic response simulation. Secondary heat conduction element DC2D8 was selected for thermal analysis. Finally, the simulation results corresponding to the peak temperature within a duration of 4 s in figure 7*B* were extracted and discussed.

Result Analysis

Figure 9 presents the simulation results for heat flow distribution at different times within asphalt pavement structure.

Heat flux field (HFL) values indicate the size of heat flow; positive values indicate the direction of heat flow is upward (heat release), whereas negative values indicate that the direction of heat flow is downward (heat

TABLE 2
Thermal characteristics parameters of the pavement structure

Parameters	SBS SMA-13	SBS AC-20	Cement Concrete	Cement Stabilized Macadam		Soil Base
Conductivity K, J/m·h·°C	4,680	4,680	6,262	5,616	5,616	5,616
Density P, kg/m^3	2,400	2,400	2,500	2,100	2,100	1,900
Specific heat C, J/kg·°C	924.9	924.9	970	911.7	911.7	1,040.0
Thermal expansion coefficient, °C^{-1}	2×10^{-5}	0.98×10^{-5}	0.98×10^{-5}	0.98×10^{-5}	0.98×10^{-5}	0.45×10^{-5}
Thickness, m	0.06	0.09	0.36	0.18	0.18	…
Absorption factor of solar radiation	0.9					
Road emissivity	0.81					
Absolute zero temperature, °C	−273					
Stefan-Boltzmann constant, J/h·m^2·K^4	2.041092×10^{-4}					

TABLE 3
Weather parameters on June 4

Area	Daily Average Maximum Temperature, °C	Daily Average Minimum Temperature, °C	Daily Average Wind Speed, m/s	t_1, h	t_2, s	Total Solar Radiation, MJ/m^2
Beijing	30	18.8	2.8	10.7	1.0	26.3×10^6

FIG. 8
The meshing model of pavement.

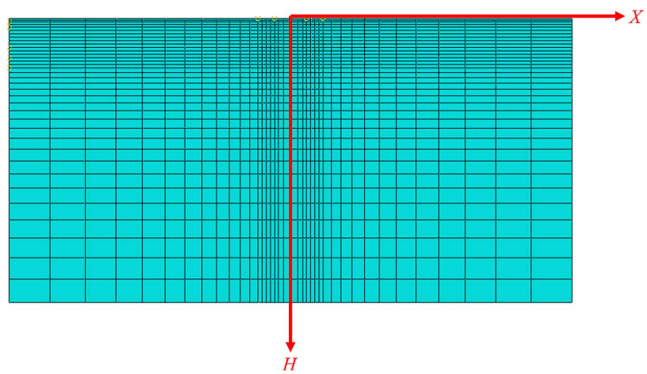

absorption). As can be seen from figure 9, the HFL value of pavement structure is positive at 1.8 s because the initial temperature of pavement is higher than the ambient temperature, which means that heat conduction transfers upward and pavement radiates heat into the environment. At 3 s, the HFL value of the pavement structure under jet wake is negative, which means that the heat conduction transfers downward and the temperature of the pavement increases because of heat absorption. At 3.8 s, the heat transfer of pavement is bidirectional, and the pavement temperature gradually decreases. At the same time, it can be seen that the change of heat flow mainly occurs in the upper layer of the pavement structure, which is relatively small at a certain depth. The temperature curves of each structural layer with time and temperature distribution of different pavement depths are shown in figure 10.

It can be seen from figure 10 that temperature at the depth of 0.4 m rises rapidly after 2.4 s and reaches the peak at 3.1 s. The maximum temperatures of pavement surface, the bottom of SMA-13 layer, and the bottom of AC-20 layer are 78.93°C at 3.1 s, 63.89°C at 3.2 s, and 47.51°C at 3.5 s, respectively. To further improve the accuracy of analysis, SMA-13, AC-20, and cement concrete layers were divided into three sublayers. The temperature of each proposed depth at 3.1 s is presented in Table 4.

FIG. 9 Heat flow distribution at different times inside pavement: (*A*) 1.8 s, (*B*) 3 s, (*C*) 3.3 s, and (*D*) 3.8 s.

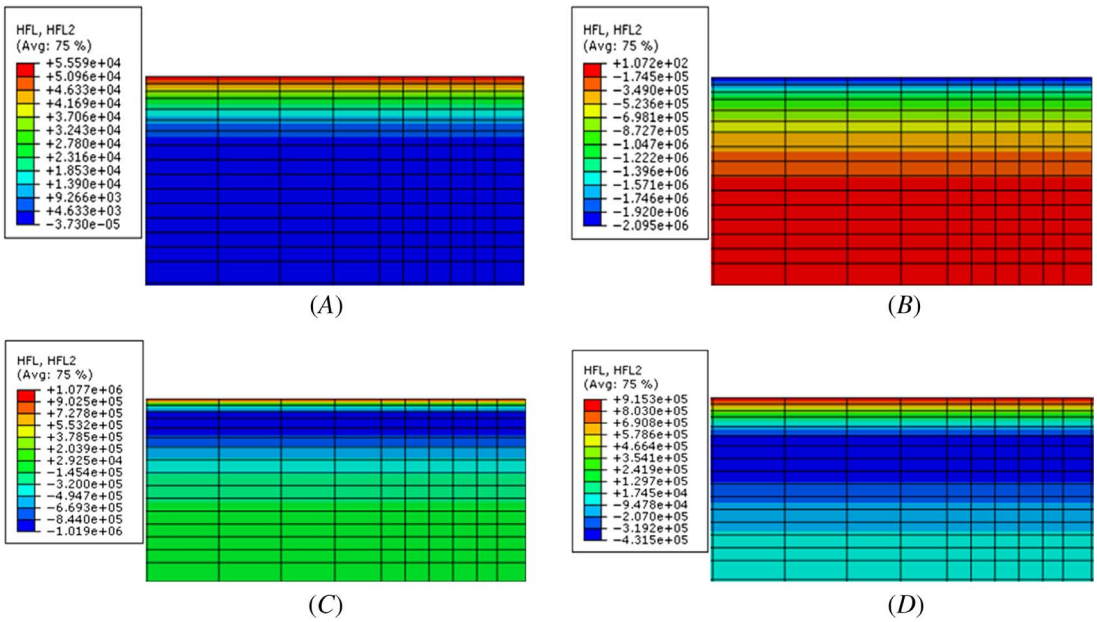

FIG. 10

Temperature distribution inside pavement: (*A*) temperature change with time; (*B*) temperature distribution at different depths.

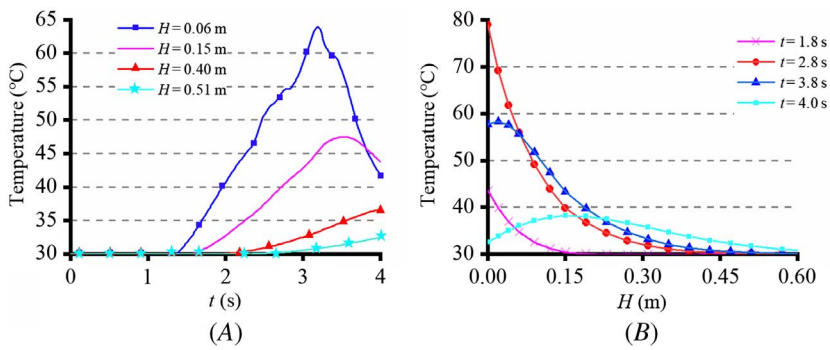

TABLE 4
The temperature distribution of each layer at 3.1 s

Material	SMA-13			AC-20			Cement Concrete		
Location	Upper	Middle	Bottom	Upper	Middle	Bottom	Upper	Middle	Bottom
H, m	0.02	0.04	0.06	0.09	0.12	0.15	0.27	0.39	0.51
T, °C	74.58	69.12	61.19	55.98	49.17	45.64	39.85	32.89	30.66

Dynamic Response Analysis

VISCOELASTIC PARAMETERS OF ASPHALT MIXTURES

Based on the dynamic modulus test, dynamic modulus at −10°C, 5°C, 20°C, 35°C, and 50°C were obtained, and the relaxation modulus could be calculated by equation (1).

$$E(t) = \frac{E'(f)}{\lambda'}; E'(f) = |E^*|\cos(\varphi) \tag{1}$$

where $|E^*|$ is dynamic modulus, $E'(f)$ is storage modulus, $E(t)$ is relaxation modulus, and λ' is the adjustment function.

Before analyzing the dynamic response of asphalt pavement in ABAQUS, the time and temperature dependence of the viscoelastic parameters should be considered in the material definition of asphalt mixtures. The time dependence could be expressed according to the sequence of the Prony series in the form of shear modulus. For an asphalt mixture, the time dependence at the selected reference temperature can be determined by the S-shape function fitted with the relaxation modulus. Then, the shift factor at each testing temperature can be determined (equation (2)). The temperature dependence could be obtained by the WLF equation, where the constants C_1 and C_2 can be calculated by equation (3).

$$a_T = \frac{t}{\xi} \tag{2}$$

$$\log(a_T) = \frac{-C_1(T - T_{ref})}{C_2 + (T - T_{ref})} \tag{3}$$

where T is the testing temperature, T_{ref} is the reference temperature, a_T is the shift factor at T_{ref}, t is the time at T before conversion, ξ is the relaxation time at the reference temperature T_{ref} after conversion, and C_1, C_2 are regression constants.

FIG. 11

Typical master of relaxation modulus.

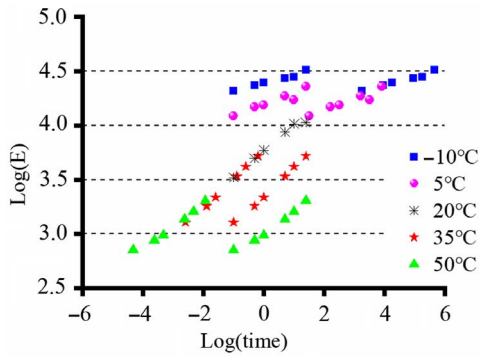

FIG. 12

The fitting result of Prony parameters.

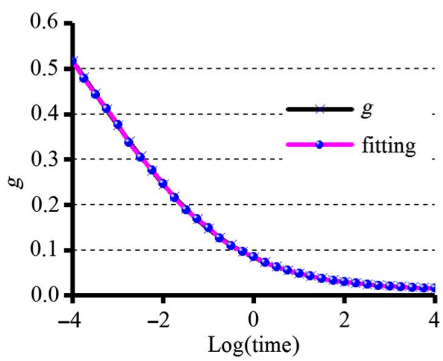

Figure 11 shows a typical master curve of relaxation modulus, and figure 12 shows the fitting result of the Prony parameters. Therefore, viscoelastic parameters of each pavement layer under the temperature field of jet wake and ambient radiation could be calculated, as given in Tables 5–7. The Prony parameters of asphalt mixture

TABLE 5
WLF equation parameters

Materials	T_{ref}, °C	C_1	C_2
SMA-13	20.0	27.8	219.8
AC-20	20.0	32.3	265.1

TABLE 6
Prony parameters of asphalt mixture at 30°C

		g_i	
T, °C	τ_i	SMA-13	AC-20
30	1.00E-05	0.38044	0.60585
	0.0001	0.13766	0.11780
	0.001	0.14686	0.10257
	0.01	0.12526	0.07085
	0.1	0.08896	0.04421
	1	0.05255	0.02444
	10	0.02855	0.01341
	100	0.01336	0.00644
	1,000	0.00992	0.00520

TABLE 7
Prony parameters of asphalt mixture at different temperatures

		g_i			g_i			g_i
T, °C	τ_i	SMA-13 Upper	T, °C	τ_i	SMA-13 Middle	T, °C	τ_i	SMA-13 Bottom
74.58	1.00E-05	0.90238	69.12	1.00E-05	0.86001	61.19	1.00E-05	0.81380
	0.0001	0.04000		0.0001	0.05805		0.0001	0.07604
	0.001	0.02354		0.001	0.03552		0.001	0.04890
	0.01	0.01131		0.01	0.01725		0.01	0.02443
	0.1	0.00619		0.1	0.00926		0.1	0.01300
	1	0.00323		1	0.00472		1	0.00653
	10	0.00191		10	0.00273		10	0.00368
	100	0.00097		100	0.00136		100	0.00182
	1,000	0.00088		1,000	0.00121		1,000	0.00159
		g_i			g_i			g_i
T, °C	τ_i	AC-20 Upper	T, °C	τ_i	AC-20 Middle	T, °C	τ_i	AC-20 Bottom
55.98	1.00E-05	0.87663	49.17	1.00E-05	0.83699	45.64	1.00E-05	0.80000
	0.0001	0.04984		0.0001	0.06422		0.0001	0.07630
	0.001	0.03192		0.001	0.04309		0.001	0.05348
	0.01	0.01640		0.01	0.02289		0.01	0.02946
	0.1	0.00905		0.1	0.01263		0.1	0.01637
	1	0.00474		1	0.00655		1	0.00849
	10	0.00277		10	0.00375		10	0.00478
	100	0.00140		100	0.00187		100	0.00235
	1,000	0.00131		1,000	0.00170		1,000	0.00210

at the reference temperature of 30°C are shown in Table 6, where τ_i is the ith specified Prony retardation time constant and g_i is the ith corresponding Prony constant. Table 7 represents the Prony parameters of asphalt mixture at different temperatures calculated from Tables 4 and 6.

DYNAMIC RESPONSE UNDER THE COUPLING OF TEMPERATURE AND LOAD

As shown in figure 13, the finite element model of the pavement structure was established in ABAQUS, the geometries of which were 10 m in length, 6 m in width, and 5 m in height, respectively. To minimize the influence of the boundary effect, 1 m was left as the transition zone in the front and back side in the z-axis direction. For the boundary conditions, normal fixed were set on four flanks and fully fixed on the bottom. The whole model consists of 102,672 elements. The parameters of the pavement structural material are the same as those of the internal pavement temperature field analysis. Table 8 gives additional parameters of asphalt pavement.

Taking B737-800 aircraft landing gear as an example, the dynamic response of airport asphalt pavement under the moving aircraft loading was simulated by ABAQUS DLOAD subroutine. The grounding footprint was simplified as a rectangular uniform load as shown in figure 14, the length and width of which was 0.4 m and 0.3 m, respectively, and the pressure magnitude is 1.47 MPa.

Result Analysis

Figures 15–17 present three directional dynamic responses of airport asphalt pavement that are due to the coupled aircraft and temperature action. Herein, two cases, i.e., the integrated temperature field that is caused by jet wake together with ambient environment, and a uniform temperature field at the reference of 30°C, were compared.

FIG. 13

Dynamic response analysis model of pavement.

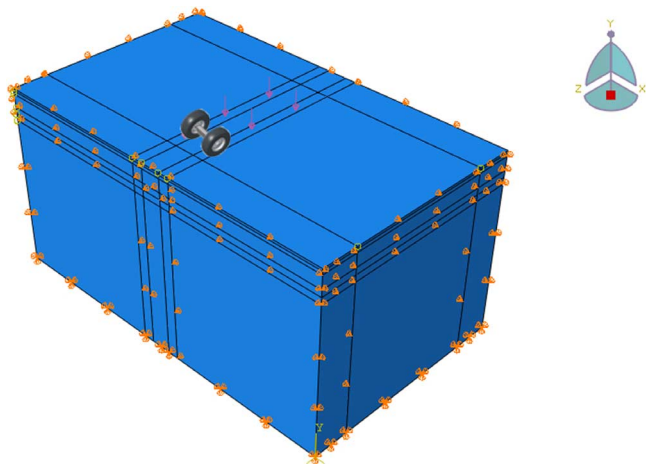

TABLE 8

Material parameters of asphalt pavement

Materials	Transient Modulus, MPa, 45°C	Poisson's Ratio	Damping Coefficient α, β
SBS SMA-13	1,750	0.35	…
SBS AC-20	2,200	0.35	…
Cement concrete	31,000	0.15	0.05
Cement stabilized macadam	2,000	0.2	0.05
Cement stabilized macadam	1,500	0.2	0.05
Soil base	30	0.4	0.05

FIG. 14 Simplified model of moving aircraft loading.

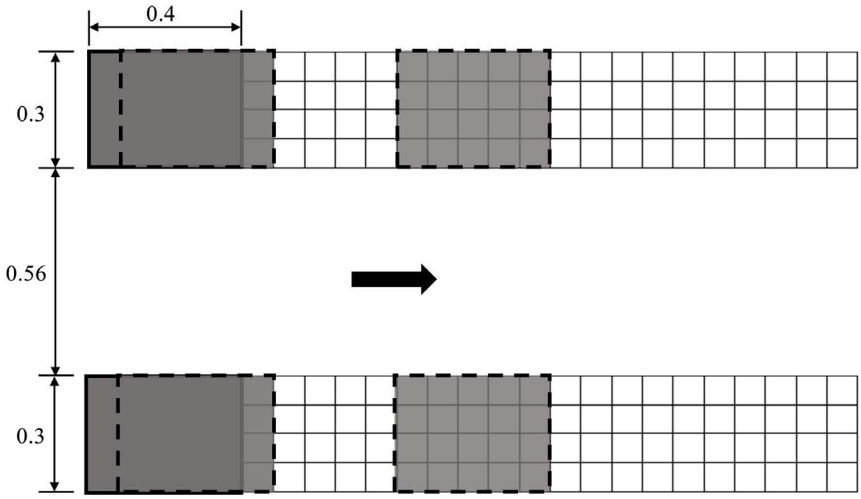

FIG. 15 Time history curve and transverse distribution of transverse strain: (*A*) time history curve; (*B*) bottom of the SMA-13 layer; (*C*) bottom of the AC-20 layer.

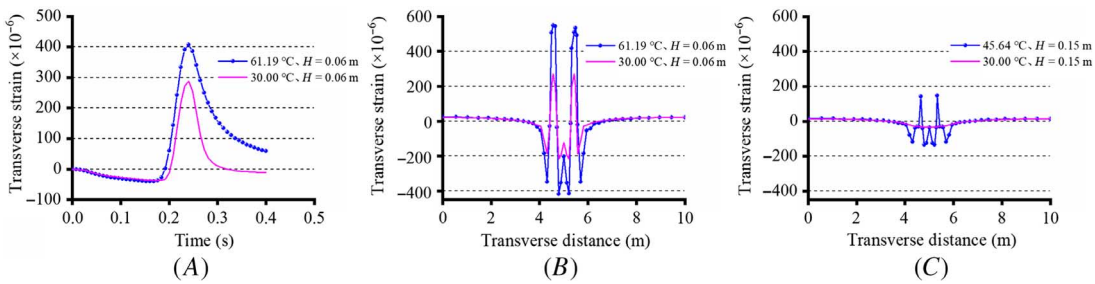

FIG. 16 Time history curve and transverse distribution of vertical strain: (*A*) time history curve; (*B*) bottom of the SMA-13 layer; (*C*) bottom of the AC-20 layer.

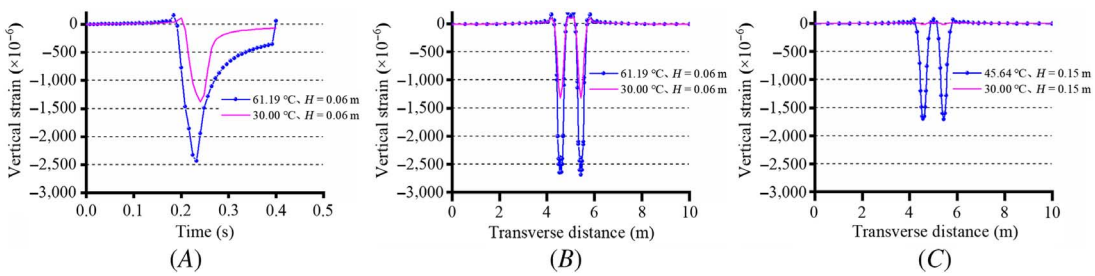

From the time history curve of transverse strain (fig. 15*A*), it can be seen that the pavement structure at both temperatures first presents slight compressive strain, which is then followed by an increase to the maximum tensile strain and then a gradual decrease. From the transverse distribution at the bottom of the SMA-13 layer

FIG. 17 Time history curve and transverse distribution of longitudinal strain: (*A*) time history curve; (*B*) bottom of the SMA-13 layer; (*C*) bottom of the AC-20 layer.

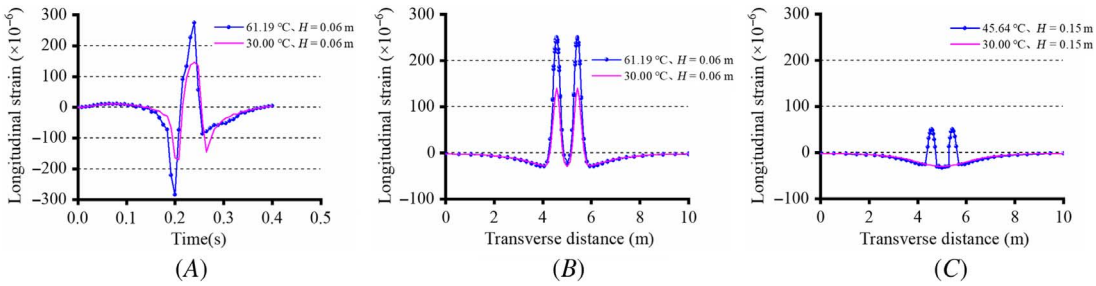

(fig. 15*B*), it can be observed that the maximum transverse tensile strain occurs at the tire footprint at both of the two temperature fields. From the transverse strain distribution at the bottom of the AC-20 layer (fig. 15*C*), it can be seen that the variation under the influence of the high-temperature jet wake is generally the same as that of the SMA-13 layer. In contrast, only a slight transverse compressive strain occurs around the tire footprint without considering the effect of jet wake. According to the results, it can be concluded that the depth range influenced by high temperature becomes larger, and the strain amplitude has the same situation. Additionally, the stress status of the AC-20 layer has been changed. Compared with 30°C, the transverse tensile strain amplitude at the bottom of the SMA-13 layer at 61.19°C is 2.14 times, whereas the transverse compressive strain amplitude is 1.53 times. More obviously, the transverse tensile strain amplitude at the bottom of the AC-20 layer is 10.8 times, and the transverse compressive strain amplitude is 3.88 times.

From the time history curve of vertical strain (fig. 16*A*), it can be seen that the pavement structure at both temperatures presents a basically opposite variation law with that of transverse strain, a slight tensile strain, followed by an increase to the maximum compressive strain and then a gradual decrease. From the transverse distribution at the bottom of the SMA-13 layer (fig. 16*B*), it can be observed that the maximum vertical compressive strain also occurs at the tire footprint at both of the two temperature fields, and the vertical tensile strain near the tire footprint is slight to negligible. From the transverse distribution at the bottom of the AC-20 layer (fig. 16*C*), it can be found that the influence of jet wake is roughly the same as that of the SMA-13 layer. In contrast, only a slight vertical compressive strain occurs near the position of the footprint without considering the effect of jet wake. According to the previous results, the vertical tensile strain amplitude at the bottom of the SMA-13 layer at 61.19°C is 1.90 times that of 30°C, whereas the vertical compressive strain amplitude is 2.03 times. More apparently, vertical tensile strain amplitude at the bottom of the AC-20 layer is 6.37 times that of 30°C, and vertical compressive strain amplitude is 98.28 times.

As seen from the time history curve of longitudinal strain (fig. 17*A*), pavement structure first presents a slight tensile strain and then reaches the maximum compressive strain and tensile strain successively. From the transverse distribution at the bottom of the SMA-13 layer (fig. 17*B*), it can be found that the maximum longitudinal tensile strain occurs at the tire footprint, and the longitudinal compressive strain near the footprint is slight to negligible. From the transverse distribution at the bottom of the AC-20 layer (fig. 17*C*), it can be observed that the variation at 45.64°C is basically the same as that of the SMA-13 layer. In contrast, only a small longitudinal compressive strain occurs near the footprint without considering the effect of jet wake. According to the results, the stress status of the AC-20 layer has been changed substantially. The longitudinal tensile strain amplitude at the bottom of the SMA-13 layer at 61.19°C is 1.78 times that at 30°C, and the longitudinal compressive strain amplitude is 1.53 times. Also, the longitudinal tensile strain amplitude at the bottom of the AC-20 layer is 10.8 times that at 30°C, and the longitudinal compressive strain amplitude is basically the same as that at 30°C. To sum up, the dynamic response of asphalt pavement subjected to the integrated temperature has been changed because of the influence of high-temperature jet wake.

FIG. 18 Maximum vertical deflection at different pavement depths: (*A*) $H = 0.00$ m, (*B*) $H = 0.06$ m, and (*C*) $H = 0.15$ m.

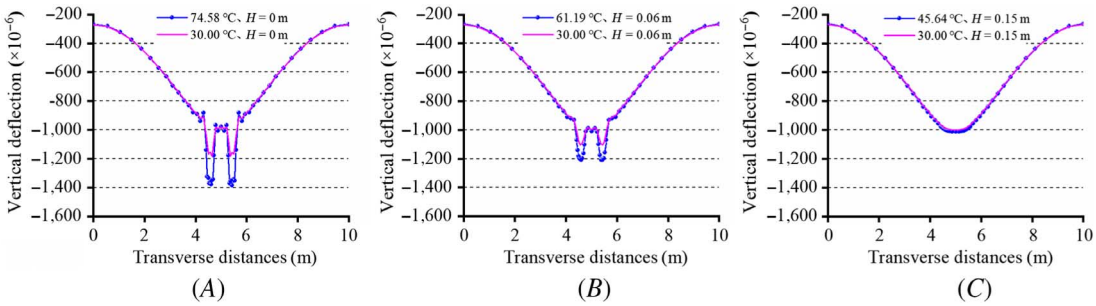

Figure 18 shows the vertical deflection at the pavement surface, the bottom of the SMA-13 layer, and the bottom of the AC-20 layer, respectively. It can be observed that the deflection at the tire footprint is the largest. On the pavement surface, the deflection at 74.58°C is 1.18 times that at 30°C and 1.09 times that at the bottom of the SMA-13 layer at 61.19°C, and the deflections at the bottom of the AC-20 layer are basically consistent.

Conclusion

Based on the sequential decoupling scheme, the temperature field distribution of high-temperature jet wake on the airport asphalt pavement and the dynamic response of the pavement structure under the coupling of temperature and aircraft load are simulated in ABAQUS. It can better reveal the actual stress state of the airport asphalt pavement. The following conclusions are drawn.

(1) The influence of high-temperature jet wake was analyzed in ABAQUS CFD platform. The results show that the temperature at the center of jet wake decreases gradually as the flow moves farther away from the nozzle, and the shape reflected on the pavement surface is similar to a parabola. The temperature on the pavement surface corresponding to the centerline of the tail nozzle is the highest and gradually decreases toward the surrounding. The temperature at the position of tire footprint could reach up to 150°C~300°C, resulting in the instant heating effect on the asphalt pavement structure being obvious and not negligible.

(2) The distribution of the temperature field inside the pavement structure was obtained by the subroutine of ABAQUS. Based on the theory of the pavement temperature field, material properties of each pavement layer calculated with the Prony series and the WLF equation are significantly different from those without considering the effect of jet wake. At the same time, it can be concluded that the high-temperature jet wake mainly affects the material properties of the asphalt concrete as the maximum temperature at the asphalt pavement surface reaches 78.93 °C and the maximum temperature at the bottom of the SMA-13 layer and AC-20 layer reaches 63.89°C and 47.51°C, respectively.

(3) Finally, comparing the proposed integrated temperature field with a uniform one, the time history curve of three directional strains shows a similar trend but with completely different amplitudes. The stress state of the SMA-13 layer is broadly similar, whereas its amplitude has increased significantly. As for the AC-20 layer, it has been changed from being subjected to only transverse compressive strain to bearing both transverse compressive strain and transverse tensile strain, as well as only longitudinal compressive strain to both longitudinal compressive strain and longitudinal tensile strain. The amplitudes of vertical compressive strain are much higher because of the heating effect of jet wake.

In conclusion, under the coupling of moving aircraft loading and integrated temperature field, asphalt pavement material is prone to developing distresses dominated by rutting, which will seriously affect the operation safety of aircraft. Therefore, the heating effect induced by high-temperature jet wake has a significant influence on the performance of pavement; thus, it is highly necessary to carry out further in-depth investigations and verifications in combination with some specific engineering project.

ACKNOWLEDGMENTS

This work was supported by the National Key R&D Program of China (No. 2018YFB1600100) and National Natural Science Foundation of China (No. 51878228). The authors would also like to acknowledge Beijing Capital International Airport Company Limited for their project support.

References

1. X.-C. Liu, L.-S. Li, X.-H. Liu, T. Zhang, X.-Y. Rong, L. Yang, and D.-Z. Xiong, "Field Investigation on Characteristics of Passenger Flow in a Chinese Hub Airport Terminal," *Building and Environment* 133 (April 2018): 51–61, https://doi.org/10.1016/j.buildenv.2018.02.009
2. J. J. Stempihar, M. I. Souliman, and K. E. Kaloush, "Fiber-Reinforced Asphalt Concrete as Sustainable Paving Material for Airfields," *Transportation Research Record* 2266, no. 1 (January 2012): 60–68, https://doi.org/10.3141/2266-07
3. P. J. Bosscher, H. U. Bahia, S. Thomas, and J. S. Russell, "Relationship between Pavement Temperature and Weather Data: Wisconsin Field Study to Verify Superpave Algorithm," *Transportation Research Record* 1609, no. 1 (January 1998): 1–11, https://doi.org/10.3141/1609-01
4. D. H. Timm, V. R. Voller, E.-B. Lee, and J. Harvey, "Calcool: A Multi-Layer Asphalt Pavement Cooling Tool for Temperature Prediction during Construction," *International Journal of Pavement Engineering* 2, no. 3 (2001): 169–185, https://doi.org/10.1080/10298430108901725
5. T. Feng and S. Feng, "A Numerical Model for Predicting Road Surface Temperature in the Highway," *Procedia Engineering* 37 (2012): 137–142, https://doi.org/10.1016/j.proeng.2012.04.216
6. J.-Q. Chen, H. Wang, and H.-Z. Zhu, "Analytical Approach for Evaluating Temperature Field of Thermal Modified Asphalt Pavement and Urban Heat Island Effect," *Applied Thermal Engineering* 113 (February 2017): 739–748, https://doi.org/10.1016/j.applthermaleng.2016.11.080
7. D. Wang, "Analytical Approach to Predict Temperature Profile in a Multilayered Pavement System Based on Measured Surface Temperature Data," *Journal of Transportation Engineering* 138, no. 5 (May 2012): 674–679, https://doi.org/10.1061/(ASCE)TE.1943-5436.0000362
8. D. Wang and J. R. Roesler, "One-Dimensional Temperature Profile Prediction in Multi-Layered Rigid Pavement Systems Using a Separation of Variables Method," *International Journal of Pavement Engineering* 15, no. 5 (2014): 373–382, https://doi.org/10.1080/10298436.2011.653358
9. D. Wang and J. R. Roesler, "One-Dimensional Rigid Pavement Temperature Prediction Using Laplace Transformation," *Journal of Transportation Engineering* 138, no. 9 (September 2012): 1171–1177, https://doi.org/10.1061/(ASCE)TE.1943-5436.0000413
10. J. Gui, P. E. Phelan, K. E. Kaloush, and J. S. Golden, "Impact of Pavement Thermophysical Properties on Surface Temperatures," *Journal of Materials in Civil Engineering* 19, no. 8 (August 2007): 683–690, https://doi.org/10.1061/(ASCE)0899-1561(2007)19:8(683)
11. C. Yavuzturk, K. Ksaibati, and A. D. Chiasson, "Assessment of Temperature Fluctuations in Asphalt Pavements Due to Thermal Environmental Conditions Using a Two-Dimensional, Transient Finite-Difference Approach," *Journal of Materials in Civil Engineering* 17, no. 4 (August 2005): 465–475, https://doi.org/10.1061/(ASCE)0899-1561(2005)17:4(465)
12. M. J. C. Minhoto, J. C. Pais, P. A. A. Pereira, and L. G. Picado-Santos, "Predicting Asphalt Pavement Temperature with a Three-Dimensional Finite Element Method," *Transportation Research Record* 1919, no. 1 (January 2005): 96–110, https://doi.org/10.1177/0361198105191900111
13. B. K. Diefenderfer, I. L. Al-Qadi, and S. D. Diefenderfer, "Model to Predict Pavement Temperature Profile: Development and Validation," *Journal of Transportation Engineering* 132, no. 2 (February 2006): 162–167, https://doi.org/10.1061/(ASCE)0733-947X(2006)132:2(162)
14. D. S. Gedafa, M. Hossain, and S. A. Romanoschi, "Perpetual Pavement Temperature Prediction Model," *Road Materials and Pavement Design* 15, no. 1 (January 2014): 55–65, https://doi.org/10.1080/14680629.2013.852610
15. Q. Xue, L. Liu, Y. Zhao, Y.-J. Chen, and J.-S. Li, "Dynamic Behavior of Asphalt Pavement Structure under Temperature-Stress Coupled Loading," *Applied Thermal Engineering* 53, no. 1 (January 2013): 1–7, https://doi.org/10.1016/j.applthermaleng.2012.10.055
16. M. U. Ahmed, A. Rahman, M. R. Islam, and R. A. Tarefder, "Combined Effect of Asphalt Concrete Cross-Anisotropy and Temperature Variation on Pavement Stress–Strain under Dynamic Loading," *Construction Building Materials* 93 (June 2015): 685–694, https://doi.org/10.1016/j.conbuildmat.2015.06.031
17. B. Ali, M. Sadek, and I. Shahrour, "Elasto-Viscoplastic Finite Element Analysis of the Long-Term Behavior of Flexible Pavements: Application to Rutting," *Road Materials and Pavement Design* 9, no. 3 (2008): 463–479, https://doi.org/10.1080/14680629.2008.9690128
18. R. Jones, D. Horner, P. Sullivan, and R. Ahlvin, "A Methodology for Quantitatively Assessing Vehicular Rutting on Terrains," *Journal of Terramechanics* 42, nos. 3–4 (July–October 2005): 245–257, https://doi.org/10.1016/j.jterra.2004.10.007
19. K. T. Hall, C. E. Correa, and A. L. Simpson, "Performance of Flexible Pavement Maintenance Treatments in the Long-Term Pavement Performance SPS-3 Experiment," *Transportation Research Record* 1823, no. 1 (January 2003): 47–54, https://doi.org/10.3141/1823-06

20. I. Pérez, L. Medina, and M. G. Romana, "Permanent Deformation Models for a Granular Material Used in Road Pavements," *Construction Building Materials* 20, no. 9 (November 2006): 790–800, https://doi.org/10.1016/j.conbuildmat.2005.01.050
21. S. C. Crow, "Stability Theory for a Pair of Trailing Vortices," *AIAA Journal* 8, no. 12 (December 1970): 2172–2179, https://doi.org/10.2514/3.6083
22. H.-F. Wang, L.-C. Cai, X.-L. Chong, and H. Geng, "Experimental Study of the Jet Engine Exhaust Flow Field of Aircraft and Blast Fences," *Promet – Traffic & Transportation* 27, no. 2 (April 2015): 181–190, https://doi.org/10.7307/ptt.v27i2.1545
23. E. Ahyudanari, N. Shafiq, and I. Kamaruddin, "Assessment Framework for Runway Pavement Distress Location," in *Recent Researches in Urban Sustainability, Architecture and Structures* (Athens, Greece: World Scientific and Engineering Academy and Society Press, 2013), 74–82.
24. F.-F. Yu, J.-B. Shi, and X.-B. Deng, "Experiments and Numerical Simulations on Temperature Field of Fighter Plane Plume," *Engineering and Testing* 51, no. 4 (2011): 31–33, https://doi.org/10.3969/j.issn.1674-3407.2011.04.008